Decentralized Algorithms for 3D Symmetric Formations in Robotic Networks – a Contraction Theory Approach

Sumeet Singh Edward Schmerling Marco Pavone

***Abstract*— This paper presents distributed algorithms for formation control of multiple robots in three dimensions. In particular, we leverage the mathematical properties of cyclic pursuit along with results from contraction and partial contraction theory to design distributed control algorithms ensuring global convergence to symmetric formations. As a base case we consider regular polygons as desired formations and then provide extensions to Johnson solid formations. Finally, we analyze the robustness of the control algorithms under bounded additive disturbances and provide performance bounds with respect to the formation error.**

I. Introduction

There has been much interest in distributed, multi-robot systems due to the plethora of possible applications and performance advantages. These systems have many attractive properties such as robustness to single-point failures, scalable implementation and potentially lower operating costs compared to monolithic approaches. Furthermore, multiple robots can together accomplish tasks which may be impossible or very difficult for any single robot on its own [1], [2], [3].

A prototypical problem in this context is distributed formation control, that is, the problem of ensuring convergence to a desired formation via control algorithms amenable to a distributed implementation [4], [5], [6]. Most of the available results consider two-dimensional formations [7], [8], [9]. Yet, a number of robotic applications would require three-dimensional (3D) formations. For example, it may be desired to deploy a set of small satellites in orbit to surround a larger damaged spacecraft to provide complete 3D reconstruction and visualization of the damaged spacecraft. Other examples include differential atmospheric, deep space, or underwater measurements [10], [11].

Accordingly, the objective of this paper is to design and rigorously analyze distributed control algorithms for 3D formations. Our approach is to leverage the simple, yet effective strategy of cyclic pursuit. Essentially, the cyclic pursuit strategy entails letting each robot i follow its leading neighbor $i+1$ modulo n, where n is the number of robots. This approach is attractive due to its decentralized nature and low information requirements; namely relative position. The cyclic-pursuit strategy for formation control has become popular in recent years due to its inherent robustness and simplicity [12], [13], [14]. In particular, we adapt the cyclic pursuit strategy proposed in [15] (that, in turn, generalizes earlier results in [13], [14]), whereby each robot follows neighbors on both sides, that is, robots $i+m$ and $i-m$ where $m = \{1,\ 2,\ \dots N\}$ counts the degree of look-ahead for each robot up to a horizon N. This is referred to as the *symmetric* cyclic control algorithm. To prove stability (i.e., convergence to a desired formation), we exploit contraction theory. Contraction theory is a relatively recent innovation in control system design [16], and hinges upon an exact differential analysis of convergence. At its core, contraction theory studies exponential convergence of pairs of system trajectories towards each other, and by extension, to a desired target trajectory. This represents a generalization with respect to traditional Lyapunov analysis, which studies convergence to the origin, i.e., to a zero trajectory [17]. Partial contraction theory extends this concept by considering the convergence of trajectories to a "set of properties," for example, a flow-invariant subspace [18], [19].

The contributions of this paper are threefold. First, we study convergence of the symmetric cyclic control algorithm to a polygon formation in 3D. Our analysis differs from the one in [15] as it considers a refined notion of the target formation (necessary to properly constraint a polygon formation). Our analysis (as the one in [15]) leverages partial contraction theory and yields insights into the various tuning parameters for the symmetric cyclic controller and their resulting effect on performance metrics such as convergence rate and control saturation. Second, we extend the definition of the target formation to be the intersection of regular polygons, thereby forming the set of strictly convex polyhedra known as Johnson solids. Control laws and sufficient conditions for convergence are derived for these relatively complex polyhedron formations, paving the way for innovative mission concepts [20]. Third, we analyze the robustness properties of the symmetric cyclic controller under bounded additive disturbances and provide performance bounds with respect to the formation error. These results provide theoretical insights for experiments performed on board the International Space Station, which highlighted the remarkable robustness properties of cyclic controllers [14].

The rest of the paper proceeds as follows: Section II introduces the mathematical background for contraction and partial contraction theory and circulant matrices which forms the basis for all subsequent analysis. Section III formalizes the problem, introduces the formation subspace and symmetric cyclic control law, and provides conditions for convergence to a regular polygon. In Section IV, we extend the results to Johnson solid formations. Section V examines robustness properties of the symmetric cyclic controller under bounded additive disturbances. Finally, in Section VI, we draw our conclusions and provide avenues for future work.

II. Mathematic Preliminaries

A. Notation

Given a square matrix A, the symmetric part of A, i.e., $(1/2)(A + A^T)$, is denoted by A_{sym}. The smallest and largest eigenvalues of A_{sym} are denoted, respectively, by $\lambda_{\min}(A)$ and $\lambda_{\max}(A)$. Accordingly, the matrix A is positive

Sumeet Singh, Edward Schmerling and Marco Pavone are with the Department of Aeronautics and Astronautics, Stanford University, Stanford, CA, 94305, {ssingh19, schmrlng, pavone @stanford.edu}

This work was supported in part by the Stanford Graduate Fellowship (SGF) and the King Abdulaziz City for Science and Technology (KACST)

definite (denoted $A \succ 0$) if $\lambda_{\min}(A) > 0$, and negative definite (denoted $A \prec 0$) if $\lambda_{\max}(A) < 0$. We will use this convention for the rest of the paper. Let I_k denote the k-by-k identity matrix. Let $A \otimes B$ denote the Kronecker product between matrices A and B. The null space of a matrix A is denoted by $\mathcal{N}(A)$. Finally, the set of eigenvalues of A will be denoted by $\lambda(A)$.

B. Contraction and Partial Contraction Theory

This section reviews basic results of nonlinear contraction theory [16], [21]. The basic stability result in contraction theory reads as follows.

Theorem II.1 (Contraction [16])**.** *Consider a general system of the form*

$$\dot{\boldsymbol{x}} = \boldsymbol{f}(\boldsymbol{x}, t), \tag{1}$$

where $\boldsymbol{x}$ is the $n \times 1$ state vector and $\boldsymbol{f}$ is a $n \times 1$ nonlinear, continuously differentiable vector function with Jacobian $\partial \boldsymbol{f}/\partial \boldsymbol{x}$. If there exists a square matrix $\Theta(\boldsymbol{x}, t)$ such that $\Theta(\boldsymbol{x}, t)^T \Theta(\boldsymbol{x}, t)$ is uniformly positive definite and the matrix

$$F := \left(\dot{\Theta} + \Theta \frac{\partial \boldsymbol{f}}{\partial \boldsymbol{x}} \right) \Theta^{-1}$$

is uniformly negative definite, then all system trajectories converge exponentially to a single trajectory. In this case, the system is said to be contracting.

A few remarks are in order. First, a matrix $\Theta(\boldsymbol{x}, t)$ is uniformly positive definite if there exists $\beta > 0$ such that $\forall \boldsymbol{x}$, $\forall t$ it holds $\lambda_{\min}(\Theta(\boldsymbol{x}, t)) \geq \beta$, and is uniformly negative definite if there exists $\beta > 0$ such that $\forall \boldsymbol{x}$, $\forall t$, $\lambda_{\max}(\Theta(\boldsymbol{x}, t)) \leq -\beta$. Second, the matrix F is referred to as the *generalized Jacobian* for system (1). Third, the matrix $M(\boldsymbol{x}, t) := \Theta(\boldsymbol{x}, t)^T \Theta(\boldsymbol{x}, t)$ is referred to as the *contraction metric*.

We next discuss partial contraction theory, which allows one to address questions more general than trajectory convergence. Consider system (1), and assume there exists a flow-invariant linear subspace $\mathcal{M} \subset \mathbb{R}^n$, i.e., a linear subspace with the property that, for all t,

$$\boldsymbol{x} \in \mathcal{M} \Rightarrow \boldsymbol{f}(\boldsymbol{x}, t) \in \mathcal{M}.$$

Assume that the dimension of $\mathcal{M}$ is p, and let $(\boldsymbol{e}_1, \ldots, \boldsymbol{e}_n)$ be an orthonormal basis of $\mathbb{R}^n$ where the first p vectors form a basis for $\mathcal{M}$. Let $\bar{U}$ be a $p \times n$ matrix whose rows are $\boldsymbol{e}_1^T, \ldots, \boldsymbol{e}_p^T$. Let $\bar{V}$ be an $(n-p) \times n$ matrix whose rows are $\boldsymbol{e}_{p+1}^T, \ldots, \boldsymbol{e}_n^T$. One can easily verify that matrix $\bar{V}$ is sub-unitary and satisfies the properties $\bar{V}^T \bar{V} + \bar{U}^T \bar{U} = I_n$, $\bar{V} \bar{V}^T = I_{n-p}$, and $\boldsymbol{x} \in \mathcal{M}$ if and only if $\bar{V} \boldsymbol{x} = \boldsymbol{0}$. We will refer to $\bar{V}$ as the projection matrix of $\mathcal{M}$. The main theorem in partial contraction theory can be stated as:

Theorem II.2 (Partial contraction [19])**.** *Consider a flow-invariant linear subspace $\mathcal{M}$ and its associated projection matrix $\bar{V}$. A particular solution $\boldsymbol{x}_p(t)$ of system* (1) *converges exponentially to $\mathcal{M}$ if the auxiliary system*

$$\dot{\boldsymbol{y}} = \bar{V} \boldsymbol{f} \left(\bar{V}^T \boldsymbol{y} + \bar{U}^T \bar{U} \, \boldsymbol{x}_p(t), t \right)$$

is contracting with respect to $\boldsymbol{y}$. If this is true for all particular solutions $\boldsymbol{x}_p$, all trajectories of system (1) will exponentially converge to $\mathcal{M}$ from all initial conditions.

Combining Theorems and II.1 and II.2, one obtains a powerful tool to ensure converge to a desired flow-invariant subspace.

Corollary II.3 (Convergence to flow-invariant subspace)**.** *A sufficient condition for global exponential convergence to $\mathcal{M}$ is*

$$\bar{V} \frac{\partial \boldsymbol{f}}{\partial \boldsymbol{x}} \bar{V}^T \prec 0, \qquad \textit{uniformly}.$$

In this paper, the subspace $\mathcal{M}$ will represent a desired symmetric formation.

Remark II.4 (Partial contraction with non-orthonormal matrices)**.** *Note that the application of partial contraction theory requires the rows of the projection matrix $\bar{V}$ to be orthonormal. However, the matrix V characterizing a subspace $\mathcal{M}$ may not be row-wise orthonormal, e.g., when it is obtained by combining a set of linearly independent equations. However, as long as the equations are independent, the matrix V will be full row-rank, Thus, it can always be transformed via an invertible transformation T into an orthonormal counterpart $\bar{V}$ which satisfies (1) $V = T\bar{V}$, (2) $\bar{V}\boldsymbol{x} = \boldsymbol{0} \Leftrightarrow \boldsymbol{x} \in \mathcal{M}$, and (3) $\bar{V} \frac{\partial \boldsymbol{f}}{\partial \boldsymbol{x}} \bar{V}^T \prec 0 \Leftrightarrow V \frac{\partial \boldsymbol{f}}{\partial \boldsymbol{x}} V^T \prec 0$ [18].*

C. Circulant and Block-Circulant Rotational Matrices

A circulant matrix of order n is a square matrix with the following structure:

$$C = \begin{bmatrix} c_1 & c_2 & \cdots & c_n \\ c_n & c_1 & \cdots & c_{n-1} \\ \vdots & \vdots & & \vdots \\ c_2 & c_3 & \cdots & c_1 \end{bmatrix} \tag{2}$$

The elements of each row are identical to the row above, but shifted one position to the right and wrapped around. Thus, a circulant matrix can be compactly denoted as:

$$C = \text{circ}[c_1 \; c_2 \; \ldots \; c_n].$$

A useful circulant matrix with dimensions $n \times n$ used in this paper is defined below:

$$L_m := \text{circ}[1, 0, \ldots, 0, \underbrace{-1}_{(m+1)\text{st element}}, 0, \ldots, 0].$$

In the following, we will denote by $\mathcal{C}_{L \otimes R}$ the set of block-circulant matrices that can be written as $L \otimes R_\beta$, where L is a circulant matrix and R_β is a rotation matrix about the axis $\boldsymbol{e}_z := (0, 0, 1)^T$ with rotation angle β. From the properties of the Kronecker product, the eigenvalues and eigenvectors of a matrix in $\mathcal{C}_{L \otimes R}$ are given, respectively, by the product of eigenvalues and Kronecker product of eigenvectors of the circulant matrix L and the rotation matrix R_β.

III. Symmetric Planar Formations

A. Problem Setup

Consider n mobile robots (uniquely labelled by an integer $i \in \{1, \ldots, n\}$). Denote the position of robot i at time t as $\boldsymbol{x}_i(t)$, where $\boldsymbol{x}_i(t) \in \mathbb{R}^3$. The overall state vector is denoted by $\boldsymbol{x} = (\boldsymbol{x}_1^T, \boldsymbol{x}_2^T, \ldots, \boldsymbol{x}_n^T)^T$. The dynamics of each robot are given by

$$\dot{\boldsymbol{x}}_i = \boldsymbol{g}_i(\boldsymbol{x}) + \boldsymbol{u}_i(\boldsymbol{x}, t), \tag{3}$$

where $\boldsymbol{u}_i$ is the control action. It is desired to design the control actions so that (1) they drive the global state vector $\boldsymbol{x}$ to a desired symmetric formation, and (2) they are amenable to a distributed implementation. As in [15], our strategy is to "encode" a symmetric formation as a "formation subspace", as discussed next. The proofs for all theorems and lemmas introduced in this section are provided in the appendix.

B. Formation Subspace

In this section we consider *regular polygons* as desired symmetric formations – the extension to non-planar formations is discussed in Section IV. Consider the case where the direction normal to the desired formation polygon is aligned with the vector $\boldsymbol{e}_z$ (the general case can be reduced to this case via a coordinate transformation). We encode such a formation via the subspace:

$$\begin{aligned}\mathcal{M}_n = \{&\boldsymbol{x} \in \mathbb{R}^{3n} : \\ &(\boldsymbol{x}_{i+1} - \boldsymbol{x}_i) = R_{2\pi/n}(\boldsymbol{x}_{i+2} - \boldsymbol{x}_{i+1}), i = 1, \dots, n-2, \quad (4a) \\ &\boldsymbol{e}_z^T(\boldsymbol{x}_n - \boldsymbol{x}_{n-1}) = \boldsymbol{e}_z^T(\boldsymbol{x}_1 - \boldsymbol{x}_n)\}, \quad (4b)\end{aligned}$$

where the indices are considered modulo n, and $R_{2\pi/n}$ denotes a counterclockwise rotation around $\boldsymbol{e}_z$. The $n-2$ constraints in (4a) will be referred to as *rotational constraints* while the single constraint in (4b) will be referred to as the *in-plane* constraint. The in-plane constraint, not considered in [15], is needed in order to ensure that all robots lie in the same plane (which is not ensured by the rotational constraints alone, one can readily find counterexamples). The following lemma shows that the constraints (4a) and (4b) are indeed necessary and sufficient for the definition of a regular polygon.

Lemma III.1 (Polygon constraints)**.** *The set of constraints* (4a) *and* (4b) *are necessary and sufficient for the definition of a regular polygon with normal direction $\boldsymbol{e}_z$. Furthermore, these constraints are linearly independent.*

In addition to the above result, consider the following corollary regarding the sufficiency of the rotational constraints for the case where two neighboring robots in the polygon are known to already lie on the desired plane.

Corollary III.2 (Reduced polygon constraints)**.** *Assume two neighboring robots j and $j+1$ are constrained to lie in the desired plane with normal $\boldsymbol{e}_z$, where the indices $\{j, j+1\} \in \{1, \dots, n\}$ are modulo n. Then the rotational constraints given in* (4a) *are necessary and sufficient for the definition of a regular polygon with normal direction $\boldsymbol{e}_z$.*

Remark III.3 (Polygon Degrees of Freedom)**.** *The constraints* (4a) *and* (4b) *together form a set of $3n-5$ linearly independent equations in $3n$ variables. The five missing equations correspond to five distinct degrees of freedom: three in translation, one in scaling, and one in in-plane rotation. That is, the polygon may be translated anywhere in space, scaled in size, or rotated within the desired plane about the plane normal.*

Both (4a) and (4b) can be compactly represented as the null space of a certain matrix, as shown in the following lemma.

Lemma III.4 (Compact constraints)**.** *Let $W_{r_n} := [I_{n-2}, 0_{(n-2)\times 2}]$ and $W_{p_n} := [0_{1\times(n-2)}, 1, 0]$. Define the $3(n-2)+1 \times 3n$ matrix*

$$V := \underbrace{\begin{bmatrix} W_{r_n} \otimes I_3 \\ W_{p_n} \otimes \boldsymbol{e}_z^T \end{bmatrix}}_{:=\mathcal{W}_n} \underbrace{(L_1 \otimes I_3 + (L_1 - L_2) \otimes R_{2\pi/n})}_{:=\mathcal{P}_n \in \mathcal{C}_{L\otimes R}}. \quad (5)$$

Then the rotational and in-plane constraints in equation (4a) *and* (4b) *are equivalent to the equation $V\boldsymbol{x} = 0$.*

Note that W_{r_n} captures the rotational constraints, while W_{p_n} captures the in-plane constraint. The subspace $\mathcal{M}_n$ can then be characterized as the null space of matrix V, that is,

$$V\,\boldsymbol{x} = \boldsymbol{0} \Leftrightarrow \boldsymbol{x} \in \mathcal{M}_n.$$

Our standing assumption throughout this paper is that the internal dynamics, i.e., $\boldsymbol{g}(\boldsymbol{x})$, are flow-invariant with respect to $\mathcal{M}_n$:

Assumption 1 (Flow invariance)**.** *The internal dynamics are flow-invariant with respect to the desired formation, that is for all $\boldsymbol{x} \in \mathcal{M}_n$ one has $V\boldsymbol{g}(\boldsymbol{x}) = \boldsymbol{0}$.*

C. Symmetric Cyclic Controller

We consider the class of symmetric cyclic controllers proposed in [15] (in turn generalizing the pursuit controllers introduced in [13]):

$$\boldsymbol{u}_i = \sum_{m=1}^{N} k_m \big[R_m(\boldsymbol{x}_{i+m} - \boldsymbol{x}_i) + R_m^T(\boldsymbol{x}_{i-m} - \boldsymbol{x}_i)\big], \quad (6)$$

where N is the look-ahead horizon ($0 < N < n-1$), $k_m > 0$ is a gain, R_m is a rotation matrix around $\boldsymbol{e}_z$ with rotation angle α_m, and $(\boldsymbol{x}_{i+m} - \boldsymbol{x}_i)$ and $(\boldsymbol{x}_{i-m} - \boldsymbol{x}_i)$ denote the relative coordinates among robot i and its $i+m$ and $i-m$ neighbors (modulo n). Note that the above control law is spatially-distributed, as each robot only requires relative position information from a set of neighboring robots.

Then, the cyclic controller can be written in compact form as

$$\begin{aligned}\boldsymbol{u} &= -\sum_{m=1}^{N} k_m \left[L_m \otimes R_m + L_m^T \otimes R_m^T\right]\boldsymbol{x} \\ &= -\sum_{m=1}^{N} k_m \mathcal{L}_m \boldsymbol{x} = -\mathcal{L}\,\boldsymbol{x}, \quad (7)\end{aligned}$$

$\mathcal{L}_m := L_m \otimes R_m + L_m^T \otimes R_m^T \in \mathcal{C}_{L\otimes R}$ and $\mathcal{L} := \sum_{m=1}^{N} k_m \mathcal{L}_m$. In order to apply partial contraction theory, the control law needs to be flow-invariant (note that, by Assumption 1, the internal dynamics are flow invariant). The next lemma shows that this is indeed the case.

Lemma III.5 (Flow invariance)**.** *Subspace $\mathcal{M}_n$ is flow-invariant with respect to the symmetric cyclic control law given in equation* (7)*.*

We are now in a position to apply partial contraction theory to show that, under some assumptions, the cyclic controller drives the system to the desired formation subspace $\mathcal{M}_n$. As the encoded constraints are linearly independent, by construction, V is full row-rank so that an invertible transformation to its orthonormal counterpart $\bar{V}$ exists.

In the following, to prove convergence to $\mathcal{M}_n$, we will apply partial contraction theory with respect to $\bar{V}$. Let $\bar{U}$ be a matrix whose rows represent an orthonormal basis for the orthogonal complement of the subspace defined by the rows of $\bar{V}$. According to Theorem II.2, we want to show that for system

$$\dot{\boldsymbol{x}} = \boldsymbol{g}(\boldsymbol{x}) - \mathcal{L}\,\boldsymbol{x},$$

the associated auxiliary system

$$\dot{\boldsymbol{y}} = \bar{V}\Big(\boldsymbol{g}(\bar{V}^T\boldsymbol{y} + \bar{U}^T\bar{U}\boldsymbol{x}_p) - \mathcal{L}\,(\bar{V}^T\boldsymbol{y} + \bar{U}^T\bar{U}\boldsymbol{x}_p)\Big),$$

is contracting. Note that by Assumption 1 and Lemma III.5 the closed-loop dynamics are invariant with respect to $\mathcal{M}_n$. Then, according to Corollary II.3, one requires

$$\bar{V}\left(\frac{\partial \boldsymbol{g}}{\partial \boldsymbol{x}} - \mathcal{L}\right)\bar{V}^T \prec 0, \qquad \text{uniformly.}$$

By Remark II.4, since V and $\bar{V}$ are related by an invertible transformation, the above stability requirement can be reformulated in terms of V directly, i.e.,

$$\mathcal{W}_n\mathcal{P}_n\left(\frac{\partial \boldsymbol{g}}{\partial \boldsymbol{x}} - \mathcal{L}\right)\mathcal{P}_n^T\mathcal{W}_n^T \prec 0, \qquad \text{uniformly.} \quad (8)$$

Performing an eigenvalue analysis of (8) (that heavily exploits the properties of circulant matrices given in Section II-C), one obtains the main result of this section.

Theorem III.6 (Polygon convergence)**.** *Assume*

$$\sup_{\boldsymbol{x},t}\left(\lambda_{\max}\left(\mathcal{P}_n\frac{\partial \boldsymbol{g}}{\partial \boldsymbol{x}}\mathcal{P}_n^T\right) - \min_{\substack{1\le i\le n\\ k\in\{-1,0,1\}}}\sum_{m=1}^{N} k_m\,\lambda_{ik}^{(m)}\right) < 0, \quad (9)$$

where

$$\lambda_{ik}^{(m)} = \frac{2}{e^{\frac{2\pi(2(i-1)+k)j}{n}}}\left[\cos(k\alpha_m) - \cos\left(k\alpha_m + \frac{2\pi m(i-1)}{n}\right)\right] \left[\left(e^{\frac{2\pi(i-1+k)j}{n}} - 1\right)\left(e^{\frac{2\pi(i-1)j}{n}} - 1\right)\right]^2.$$

Then system (3) *under the cyclic controller* (6) *globally converges to a symmetric formation, i.e., to the formation subspace* $\mathcal{M}_n$.

Due to the needed inclusion of in-plane constraint, the eigenvalues in Theorem III.6 differ from those in [15].

For a given number of robots, the primary design parameters in the cyclic controller include the gains k_m and the look-ahead horizon N. It is clear that increasing the gains uniformly scales all eigenvalues of the projected Jacobian, thereby increasing the exponential convergence rate. However, this is at the expense of a more aggressive controller which increases the risk of saturating the controller. On the other hand, increasing the look-ahead horizon, while imposing greater information requirements for each robot, also increases the convergence rate but at a lower risk of control saturation. This is due to the fact that the net control action generated is dependant on the asymmetry between the forward and rear neighbors of each robot. Thus, instead of directly scaling the controller via the gains which undoubtedly increases the control magnitude by the scale factor, one can take advantage of the increased convergence rate with a larger horizon, with comparatively modest increases in control effort. The appendix presents a simulation result exemplifying this intuition.

Remark III.7 (Formations of fixed size)**.** *If* $\alpha_m = m\pi/n$ *then the formation converges to a regular polygon with fixed, but unspecified size. This can be shown by noting that the forward and rear components of the cyclic controller cancel for* $\boldsymbol{x} \in \mathcal{M}_n$ *and* $\alpha_m = m\pi/n$.

Remark III.8 (Double integrator dynamics)**.** *Assuming zero internal dynamics (i.e.,* $\boldsymbol{g}(\boldsymbol{x}) = \boldsymbol{0}$*), the symmetric cyclic control law can easily be extended to double integrator dynamics by augmenting the control law as follows:*

$$\begin{aligned}\boldsymbol{u}_i =& k_d\sum_{m=1}^{N} k_m\big[R_m(\boldsymbol{x}_{i+m}-\boldsymbol{x}_i)+R_m^T(\boldsymbol{x}_{i-m}-\boldsymbol{x}_i)\big]+\\ &\sum_{m=1}^{N} k_m\big[R_m(\boldsymbol{v}_{i+m}-\boldsymbol{v}_i)+R_m^T(\boldsymbol{v}_{i-m}-\boldsymbol{v}_i)\big] - k_d\boldsymbol{v}_i\,,\end{aligned}$$

where $k_d > 0$ *is a constant gain,* $\boldsymbol{u}$ *now represents the acceleration control command and* $\boldsymbol{v}$ *represents robot velocities. The control law remains spatially-distributed in terms of relative velocities with the addition of a feedback term on absolute velocity. Convergence analysis for the system can be carried out by introducing an auxiliary variable* $\boldsymbol{s}_i = k_d\boldsymbol{x}_i + \boldsymbol{v}_i$ *which satisfies the circulant equation:* $\dot{\boldsymbol{s}} = \mathcal{L}\boldsymbol{s}$*. Then, provided the system in terms of this auxiliary variable* $\boldsymbol{s}$ *is contracting to the desired subspace, the trajectories* $\boldsymbol{x}$*, of the robots are the output of the first order system* $\dot{\boldsymbol{x}} + k_d\boldsymbol{x} = \boldsymbol{s}$.

Remark III.9 (General plane of convergence)**.** *In the scenario where the desired formation plane is not the horizontal plane, a similarity transformed version of the control rotation matrix* R_m *should be used. For consistency, let* $\boldsymbol{e}_z$ *remain the desired plane normal in a rotated frame defined by the rotation matrix* R_η*. Define* R_{m_s} *to represent the similarity transformed version of* R_m*, i.e.,*

$$R_{m_s} = R_\eta^T R_m R_\eta.$$

Then, the rotation matrix R_m *in (6) can be replaced by* R_{m_s}*. Accordingly, the cyclic controller in (7) becomes:*

$$\begin{aligned}\boldsymbol{u} &= -\underbrace{(I_n\otimes R_\eta^T)}_{:=\mathcal{R}_\eta^T}\sum_{m=1}^{N} k_m\mathcal{L}_m\underbrace{(I_n\otimes R_\eta)}_{:=\mathcal{R}_\eta}\boldsymbol{x}\\ &= -\sum_{m=1}^{N} k_m\mathcal{L}_{m\eta}\boldsymbol{x} = -\mathcal{L}_\eta\boldsymbol{x},\end{aligned} \quad (10)$$

where $\mathcal{L}_{m\eta} := \mathcal{R}_\eta^T\mathcal{L}_m\mathcal{R}_\eta$ *and* $\mathcal{L}_\eta := \sum_{m=1}^{N} k_m\,\mathcal{L}_{m\eta}$*. The expression for the projection matrix* V *becomes:*

$$V = \mathcal{W}_n\mathcal{P}_n\mathcal{R}_\eta. \quad (11)$$

These modifications do not affect convergence analysis, but will be instrumental for the extension to Johnson solid formations in Section IV.

Figure 1a demonstrates the use of the symmetric cyclic controller with 6 robots. The robots were randomly initialized around the point $(1,1,1)^T$ with a look-ahead horizon $N = 2$ and a desired formation plane tilted 42^o from the vertical. In addition to cyclic control, the robots were also subject to an additional decentralized controller that allowed the formation to converge to a specific size with a desired geometric center. The control was implemented in two phases whereby the robots were first allowed to converge to a regular polygon before a flow-invariant controller was switched on to separate the robots to a desired distance and shift the geometric center to the origin. This switch can clearly be noted in Figure 1b which plots the inter-robot distances with respect to robot 1. The analysis for this switching controller is presented in the Appendix.

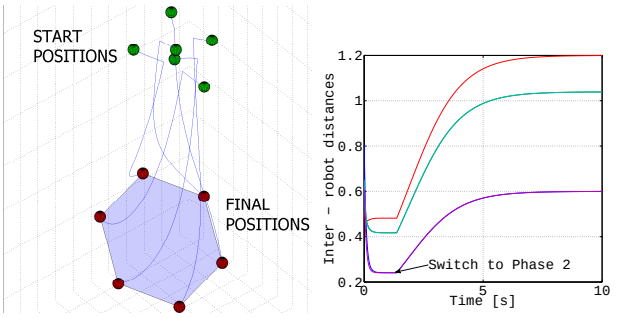

(a) 3D Trajectory with size and center control.

(b) Inter-robot distances for Robot 1. Desired neighbor separation: 0.6.

Fig. 1: Single planar formation simulation.

IV. Polyhedral Formations

In this section we extend the results of Section III to *polyhedral formations*. Specifically, we focus on convex polyhedra having regular faces and equal edge lengths, referred to as Johnson solids. The main idea is to associate each face of a polyhedron with a set of robots equal to the number of vertices of that face, see Figure 2.

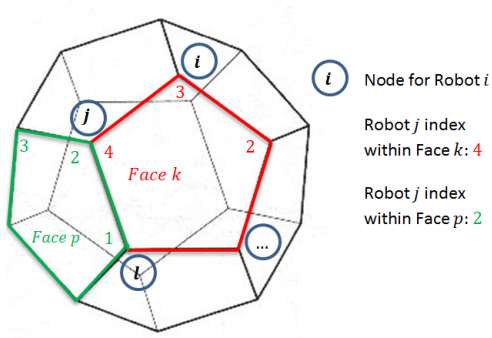

Fig. 2: General polyhedron notation.

Specifically, let $\mathcal{A}$ be the set of robots, let $\mathcal{F}$ be the set of faces in the Johnson polyhedron, and let $\mathcal{F}_k$ be its kth face. Furthermore, let $\mathcal{V}_k$ be the set of vertices of face $\mathcal{F}_k$ and let $\boldsymbol{n}_k$ be the unit outward normal of face $\mathcal{F}_k$ (pointing outward from the interior of the polyhedron). Let the number of robots n be equal to the number of vertices in the polyhedron. Each robot is *uniquely* associated with a vertex in the polyhedron. Each face induces a sub-indexing of the robots, specifically, let i_k denote the index of robot i in face k, where $i = 1, \dots, n$ and $k = 1, \dots, |\mathcal{F}|$, see Figure 2. If robot i does not belong to face k, then we use the convention $i_k = \infty$. For consistency, we assume a counter-clockwise index assignment within a face, where the counter-clockwise direction is with respect to the outward normal $\boldsymbol{n}_k$.

In order to study convergence using partial contraction theory, we require a non-redundant characterization of the polyhedron. In particular, we consider a strict subset of $L < |\mathcal{F}|$ faces that are sufficient to fully constrain the formation. Without loss of generality, assume that the set of these L faces, which we will call $\mathcal{F}_L$, is the first L faces in $\mathcal{F}$. The faces in $\mathcal{F}_L$ *uniquely* identify a Johnson polyhedron and will be referred to as the basis faces of $\mathcal{F}$. Prior to a discussion on how this subset of faces is chosen, we first introduce some necessary notation.

For notational convenience, for each face $k = 1, \dots, L$, define the matrix $\bar{E}^{(k)} \in \mathbb{R}^{|\mathcal{V}_k| \times n}$ as

$$[\bar{E}^{(k)}]_{ij} = \begin{cases} 1 & \text{if } j_k = i, \\ 0 & \text{otherwise.} \end{cases} \tag{12}$$

Thus $[\bar{E}^{(k)}]_{ij}$ equals one if robot j's index within face k is equal to i. Then, the state of all the robots in face k can be compactly written as

$$\boldsymbol{x}^{(k)} = \left(\bar{E}^{(k)} \otimes I_3\right) \boldsymbol{x} = E^{(k)} \boldsymbol{x}, \tag{13}$$

where $\boldsymbol{x}$ is the global state vector and $E^{(k)} := \bar{E}^{(k)} \otimes I_3$ acts to permute subsets of the global state vector into a counter-clockwise arrangement of robots for face k.

Let each face in the polyhedron (by assumption a regular polygon) be described by a subspace $\mathcal{M}^{(k)}_{|\mathcal{V}_k|}$, defined in a way analogous to the one in Section III-B, as

$$\mathcal{M}^{(k)}_{|\mathcal{V}_k|} = \{\boldsymbol{x}^{(k)} \in \mathbb{R}^{3|\mathcal{V}_k|} :$$

$$R_{\eta_k}(\boldsymbol{x}^{(k)}_{i+1} - \boldsymbol{x}^{(k)}_i) = R_{2\pi/n} R_{\eta_k}(\boldsymbol{x}^{(k)}_{i+2} - \boldsymbol{x}^{(k)}_{i+1}), \quad i = 1, \dots, |\mathcal{V}_k| - 2, \tag{14a}$$

$$\boldsymbol{e}_z^T R_{\eta_k}(\boldsymbol{x}^{(k)}_{|\mathcal{V}_k|} - \boldsymbol{x}^{(k)}_{|\mathcal{V}_k|-1}) = \boldsymbol{e}_z^T R_{\eta_k}(\boldsymbol{x}^{(k)}_1 - \boldsymbol{x}^{(k)}_{|\mathcal{V}_k|})\}, \tag{14b}$$

where R_{η_k} is a rotation matrix that defines a coordinate frame with its $\boldsymbol{e}_z$ axis aligned with the outward face normal $\boldsymbol{n}_k$. According to Lemma III.4, $\mathcal{M}^{(k)}_{|\mathcal{V}_k|}$ can be represented as the null space of a $3(|\mathcal{V}_k| - 2) + 1 \times 3n$ matrix, denoted by $\tilde{V}^{(k)}$. In other words, $\boldsymbol{x} \in \mathcal{M}^{(k)}_{|\mathcal{V}_k|} \Leftrightarrow \tilde{V}^{(k)} \boldsymbol{x} = \boldsymbol{0}$.

The desired Johnson polyhedral formation can then be represented as a subspace $\mathcal{M}_n$ given by the intersection of the subspaces corresponding to the basis faces, that is

$$\mathcal{M}_n = \cap_{k=1}^{L} \mathcal{M}^{(k)}_{|\mathcal{V}_k|}. \tag{15}$$

Alternatively, the desired Johnson polyhedral formation can be represented as the intersection of null spaces $\cap_{k=1}^{L} \mathcal{N}(\tilde{V}^{(k)})$. Using (11) and (13), one can write $\tilde{V}^{(k)}$ as

$$\tilde{V}^{(k)} = \mathcal{W}_{|\mathcal{V}_k|} \mathcal{P}_{|\mathcal{V}_k|} \mathcal{R}_{\eta_k} E^{(k)}. \tag{16}$$

Having established the description of the Johnson polyhedron as the intersection of the subspaces corresponding to the basis faces set $\mathcal{F}_L$, we now discuss how to select this subset within $\mathcal{F}$. First, we state the following extension of Remark III.3:

Remark IV.1 (Normal Parity)**.** *For two polygons with linearly independent normals that share a common edge, the in-plane rotational degrees of freedom reduce to two realizations corresponding to inward versus outward facing normals in the convex hull of the two polygons. This parity is captured by the scaling degree of freedom: if the robots' position vector $\boldsymbol{x}$ lies in the intersection of the null-spaces for the two polygons and produces outward normals, then the alternate solution $-\boldsymbol{x}$ produces inward normals.*

We now present sufficient conditions for a basis face set:

Lemma IV.2 (Representation of a Johnson Polyhedron)**.** *Assume that a basis set $\mathcal{F}_L$ of a Johnson polyhedron satisfies the following three properties:*

1) *Each face within $\mathcal{F}_L$ is a regular polygon described by the nullspace of the matrix $\tilde{V}^{(k)}$ where $\tilde{V}^{(k)}$ is as given in* (16)*.*

2) *Within the dual graph of the Johnson polyhedron, the sub-graph induced by $\mathcal{F}_L$ is a tree.*
3) *The faces in $\mathcal{F}_L$ span all vertices.*

Then, $\mathcal{F}_L$ in conjunction with (15) *uniquely characterizes a Johnson polyhedron up to normal parity.*

Proof. We begin with the first assumption. From Lemma III.1 and Remark III.3, we know that each $\tilde{V}^{(k)}$ constrains the plane normal and shape of a regular polygon spanned by the vertex set $\mathcal{V}_k$.

Let us now consider two adjacent faces within $\mathcal{F}_L$. From Remark IV.1, these two faces must have a fixed orientation in space up to normal parity. For any other face $\mathcal{F}_k \in \mathcal{F}_L$, by assumption 2, there exists a unique path in $\mathcal{F}_L$ between $\mathcal{F}_k$ and these two faces. Given the normal parity fixed by the initial two faces, the orientation of $\mathcal{F}_k$ is fixed by applying Remark IV.1 along this path. Thus the mutual orientation of all faces in $\mathcal{F}_L$ is fixed.

Finally, by assumption 3, each vertex in the polyhedron belongs to at least one of the faces in $\mathcal{F}_L$. Then, the convex hull of the vertices is the desired polyhedron. □

Given our representation of the polyhedron in terms of the basis faces set, we can now combine (15) and (16) to form the global constraint matrix $\tilde{V}$:

$$\tilde{V} := \begin{bmatrix} \tilde{V}^{(1)^T} & \tilde{V}^{(2)^T} & \dots & \tilde{V}^{(L)^T} \end{bmatrix}^T. \tag{17}$$

Thus, we can compactly characterize the global desired formation subspace $\mathcal{M}_n$ as the null space of $\tilde{V}$, i.e.,

$$\boldsymbol{x} \in \mathcal{M}_n \Leftrightarrow \tilde{V}\boldsymbol{x} = \mathbf{0}.$$

As constructed, $\tilde{V}$ is not full row-rank as there are redundant constraints. Since stability analysis using partial contraction is contingent upon a full row-rank projection matrix, we propose a reduction of $\tilde{V}$ that discards redundant constraints in the $\tilde{V}^{(k)}$. To simplify the exposition, we use a labelling convention for the tree of faces $\mathcal{F}_L$, where all basis faces along the unique path between $\mathcal{F}_1$ and any $\mathcal{F}_j \in \mathcal{F}_L$ have indices less than j.

We now propose the following structure for the sub-blocks:

$$V^{(k)} = \begin{cases} \tilde{V}^{(k)} & \text{if } k = 1, 2, \\ (W_{r_{|\mathcal{V}_k|}} \otimes I_3)\mathcal{P}_{|\mathcal{V}_k|}\mathcal{R}_{\eta_k} E^{(k)} & k = 3, \dots, L, \end{cases} \tag{18}$$

where, as defined in Lemma III.4, $W_{r_{|\mathcal{V}_k|}} = [I_{|\mathcal{V}_k|-2}, 0_{(|\mathcal{V}_k|-2)\times 2}]$. That is, in-plane constraints have been removed from all but two (adjacent) faces within $\mathcal{F}_L$, specifically, $\mathcal{F}_1$ and $\mathcal{F}_2$. The following Lemma proves that the reduced constraints that stem from (18) are equivalent to the original set of constraints using $\tilde{V}^{(k)}$, and that the resulting global constraint matrix is full row-rank. The proof is provided in the appendix.

Lemma IV.3 (Minimal representation of V)**.** *Denote the set of equations $\tilde{V}^{(k)}\boldsymbol{x} = \mathbf{0}$ where $\tilde{V}^{(k)}$ has the form given in* (16) *for $k = 1, \dots, L$ as the full-constraint set. Similarly, denote the set of equations $V^{(k)}\boldsymbol{x} = \mathbf{0}$ where $V^{(k)}$ has the form given in* (18) *as the reduced-constraint set. Then, the solutions to the two sets of equations are identical. That is,*

$$\boldsymbol{x} \in \mathcal{M}_n \Leftrightarrow V\boldsymbol{x} = \mathbf{0}.$$

where $V = \begin{bmatrix} V^{(1)^T} & \dots & V^{(L)^T} \end{bmatrix}^T$. Furthermore, V is full row-rank.

Remark IV.4 (Polyhedron Degrees of freedom)**.** *Note that V has a total of $\left(3\sum_{k=1}^{L}|\mathcal{V}_k| - 6L + 2\right)$ linearly independent equations for a total of $\left(3\sum_{k=1}^{L}|\mathcal{V}_k| - 6L + 6\right)$ variables. Three degrees of freedom correspond to the three translational degrees of freedom. The final degree of freedom corresponds to scaling the polyhedron by some constant $\alpha \in \mathbb{R}$. Applying a negative scaling factor may be interpreted as flipping the entire formation — see normal parity, Remark IV.1.*

Having characterized the desired formation as the null space of a full row rank matrix, we turn our attention to the control law for each robot. Similarly to Section III-C, we consider the control law for robot i stemming from face k, that is $\boldsymbol{u}_i^{(k)}$, the cyclic controller

$$\boldsymbol{u}_i^{(k)} = \sum_{m=1}^{N_k} k_m^{(k)}\left[R_{m_s}^{(k)}(\boldsymbol{x}_{i+m}^{(k)} - \boldsymbol{x}_i^{(k)}) + R_{m_s}^{(k)^T}(\boldsymbol{x}_{i-m}^{(k)} - \boldsymbol{x}_i^{(k)})\right], \tag{19}$$

where $N_k < |\mathcal{V}_k| - 1$ is the look-ahead horizon for face k, $k_m^{(k)} > 0$ is a gain, $R_{m_s}^{(k)} = R_{\eta_k}^T R_m^{(k)} R_{\eta_k}$ with $R_m^{(k)} = R_{m\pi/|\mathcal{V}_k|}$, and $\boldsymbol{x}_{i+m}^{(k)}$ and $\boldsymbol{x}_{i-m}^{(k)}$ are neighboring robots within face k (modulo $|\mathcal{V}_k|$). The choice $R_m^{(k)} = R_{m\pi/|\mathcal{V}_k|}$ stems from the requirement that robots converge to a polygon of fixed size within each face (see Remark III.7).

The net control for each robot is then given by the superposition of contributions for each face in which the robot is present, i.e.,

$$\boldsymbol{u}_i = \sum_{k:i_k \neq \infty}^{L} \boldsymbol{u}_i^{(k)}, \qquad i = 1, \dots, n. \tag{20}$$

Using (19) and (10), the overall cyclic control vector stemming from face k is given by

$$\boldsymbol{u}^{(k)} = -\sum_{m=1}^{N_k} k_m^{(k)}\,\mathcal{L}_{m\eta}^{(k)}\boldsymbol{x}^{(k)} := -\mathcal{L}_\eta^{(k)} E^{(k)}\boldsymbol{x},$$

where $\mathcal{L}_{m\eta}^{(k)} = \mathcal{R}_{\eta_k}^T \mathcal{L}_m^{(k)} \mathcal{R}_{\eta_k}$ and $\mathcal{L}_m^{(k)} = L_m \otimes R_m^{(k)} + L_m^T \otimes R_m^{(k)^T}$. This allows us to express the contribution to the global control vector due to face k as

$$\boldsymbol{u}_k = E^{(k)^T}\boldsymbol{u}^{(k)} = -E^{(k)^T}\mathcal{L}_\eta^{(k)} E^{(k)}\boldsymbol{x}.$$

Thus, the overall closed-loop dynamics are given by

$$\dot{\boldsymbol{x}} = \sum_{k=1}^{L} \boldsymbol{u}_k(\boldsymbol{x}). \tag{21}$$

Note that, for simplicity, we are considering zero internal dynamics. A sufficient condition for convergence to the desired formation, i.e., to the subspace $\mathcal{M}_n$, is provided by the following theorem.

Theorem IV.5 (Polyhedron Convergence)**.** *Assume*

$$J = \left[V\left(\sum_{k=1}^{L} -E^{(k)^T}\mathcal{L}_\eta^{(k)} E^{(k)}\right)V^T\right] \prec 0. \tag{22}$$

Then, the closed-loop dynamics (21) *globally converge to a Johnson polyhedral formation, i.e., to the formation subspace $\mathcal{M}_n$.*

Proof. Let $\bar{V}$ represent the orthonormal counterpart of V, whose existence is guaranteed given the results of Lemma IV.3. First, we need to show that the dynamics (21) are flow invariant. Indeed, as an immediate consequence of Remark III.7 and the fact that the the rotation angle is set equal to $m\pi/|\mathcal{V}_k|$, one has

$$\boldsymbol{x} \in \mathcal{M}_n \Rightarrow \boldsymbol{u}_k(\boldsymbol{x}) = \mathbf{0}, \qquad \text{for all } k = 1, \dots, L, \quad (23)$$

and hence $\boldsymbol{x} \in \mathcal{M}_n \Rightarrow \bar{V} \sum_{k=1}^{L} \boldsymbol{u}_k(\boldsymbol{x}) = \mathbf{0}$, i.e., dynamics (21) are flow invariant.

Consider, then, the following auxiliary system for system (21):

$$\dot{\boldsymbol{y}} = \bar{V} \left(\sum_{k=1}^{L} -E^{(k)^T} \mathcal{L}_{\eta}^{(k)} E^{(k)} \left(\bar{V}^T \boldsymbol{y} + \bar{U}^T \bar{U} \boldsymbol{x}_p \right) \right).$$

Since the dynamics are flow invariant, and an invertible transformation exists between V and $\bar{V}$, then by Remark II.4 and by applying Corollary II.3, one obtains the claim. □

Remark IV.6. *Note that the condition given in* (22) *is markedly more complex than* (9)*, required for convergence to a single plane. In particular, we now have the addition of cross-terms in the projected Jacobian due to the interaction between the various faces. Additionally, when working with the auxiliary system, we did not leverage the results of flow-invariant subspaces as they were introduced in Section III. This is because if the global state vector $\boldsymbol{x}$ converges to one of the subspaces defined by $V^{(k)}$, then the global dynamics will not necessarily be flow-invariant with respect to the given face or any other faces in $\mathcal{M}_n$. This is due to two reasons: 1) Only the rotational set of constraints are used to define faces other than the ones indexed by $k = 1$ and $k = 2$, which we know are insufficient on their own to describe a regular planar polygon and 2) the cyclic control law for each robot as defined in* (20) *introduces coupling between various faces. Thus, convergence is predicated on the decay of the symmetric cyclic controller to zero for all faces.*

Figure 3 shows simulation results demonstrating convergence to complex 3D formations. The subset of faces chosen to derive the control laws $\mathcal{F}_L$, are shaded in red while all other faces are shaded in blue to indicate a closed polyhedron formation.

A potential issue to note here is the resulting effect on the system performance in the event of local robot failures. In the regular polygon case, a single point of failure simply requires the robots to reinitialize their indices within the group and subsequently converge to a smaller polygon. In the polyhedron case however, this can be problematic if the failed robot is coupled to multiple faces. In this scenario, a global restart may be required with a new polyhedron configuration that fits the reduced set of robots.

V. Robustness Analysis

In this section we discuss the robustness properties of the cyclic closed-loop dynamics (7) subject to additive disturbances. Robustness performance is measured as the Euclidean norm of the deviation of the perturbed system trajectory from the nominal contracting trajectory, with respect to the metric $\bar{V}^T\bar{V}$, where $\bar{V}$ is the orthonormal counterpart of the nominal projection matrix as defined in (5). The analysis presented in this section is restricted to zero internal

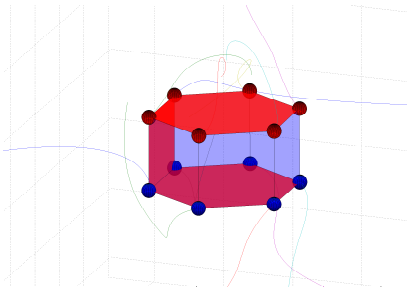

(a) Hexagon Box Formation - 12 robots

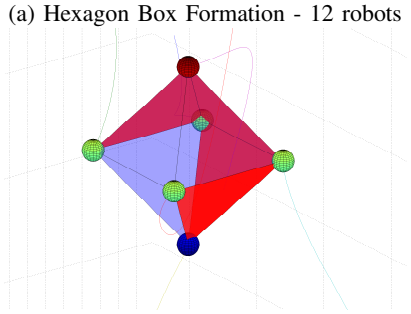

(b) Octahedron Formation - 6 robots

Fig. 3: Convergence to complex 3D formations.

dynamics (i.e., $\boldsymbol{g}(\boldsymbol{x}) = \mathbf{0}$) and to convergence to regular polygons. An analogous proof can be constructed for the Johnson polyhedron case.

Let $\boldsymbol{z}_0(t) = \bar{V}\boldsymbol{x}_0(t)$ represent the dynamics of the unperturbed system under the action of the symmetric cyclic controller (7). Then,

$$\dot{\boldsymbol{z}}_0(t) = -\bar{V}\mathcal{L}\boldsymbol{x}_0(t). \quad (24)$$

Consider the perturbed dynamics $\boldsymbol{z}_d(t)$, under an additive state and/or time dependent disturbance:

$$\dot{\boldsymbol{z}}_d(t) = -\bar{V}\mathcal{L}\boldsymbol{x}_d(t) + \boldsymbol{d}(\boldsymbol{x}_d, t). \quad (25)$$

Here the disturbance is measured in the transformed $\boldsymbol{z}$ coordinates. Let $\boldsymbol{\delta}(t)$ represent the difference between the nominal and perturbed trajectories at time t. Specifically, let $\boldsymbol{\delta}_{\boldsymbol{z}}(t) := \boldsymbol{z}_d(t) - \boldsymbol{z}_0(t)$ and $\boldsymbol{\delta}_{\boldsymbol{x}}(t) := \boldsymbol{x}_d(t) - \boldsymbol{x}_0(t)$. Note that both $\boldsymbol{\delta}_{\boldsymbol{z}}$ and $\boldsymbol{\delta}_{\boldsymbol{x}}$ equal $\mathbf{0}$ at $t = 0$ as the trajectories are assumed to start from the same point. Then,

$$\dot{\boldsymbol{\delta}}_{\boldsymbol{z}}(t) = -\bar{V}\mathcal{L}\,\boldsymbol{\delta}_{\boldsymbol{x}}(t) + \boldsymbol{d}(\boldsymbol{x}_d, t). \quad (26)$$

Let $\bar{R}^2(t) := \boldsymbol{\delta}_{\boldsymbol{z}}^T(t)\boldsymbol{\delta}_{\boldsymbol{z}}(t)$; $\bar{R}$ represents the Euclidean distance of the perturbed trajectory from the nominal one in the transformed coordinates, referred to as the *formation error*. The following theorem characterizes the robustness of cyclic pursuit. The proof is provided in the appendix.

Theorem V.1 (Cyclic Control Robustness)**.** *Assume that the nominal system is contracting with contraction rate $\Lambda = -\lambda_{\min}\left(\bar{V}\mathcal{L}\bar{V}^T\right) < 0$ and that the disturbance is norm bounded with upper bound $\bar{d}$. Then the formation error in the transformed $\boldsymbol{z}$ coordinates, that is $\bar{R}$, is upper bounded as*

$$\bar{R}(t) \leq \frac{\bar{d}}{\Lambda}(e^{\Lambda t} - 1). \quad (27)$$

Remark V.2. *The bound $\bar{R}(t)$ describes the time-varying deviation from a nominal contracting trajectory. In the limit $t \to \infty$, the steady state bound $\bar{R}_{ss} = \bar{d}/|\Lambda|$ provides a measure of the steady-state formation error. Physically, it represents a bound on the degree of asymmetry at each node*

of the formation measured by the set of linear constraints used to derive the subspace, that is, (4a) *and* (4b)*. The inverse proportionality between $\bar{R}_{ss}$ and $|\Lambda|$ highlights a potential trade-off between increased robustness, and control saturation (k_m) and/or sensor requirements (N).*

Figure 4 provides insights into the tightness of the bound. Here, perturbation was introduced into the system via error in the control rotation angles. The rotation angle in R_m for robot i is equal to $\tilde{\alpha}_i(t) = \alpha_0 + \delta_{\alpha_i}(t)$ where $\alpha_0 = m\pi/n$ is the nominal control angle and $\delta_{\alpha_i}(t)$ is a perturbation, sampled randomly from a uniform distribution over the range $\pm 1^\circ$. The plotted curves in Figure 4a correspond to the actual formation error $\bar{R}$, the Gronwall bound in (27) and a tighter bound governed by the following differential inequality (derived in the proof for Theorem V.1):

$$\dot{\bar{R}} \leq \Lambda \bar{R} + \|\boldsymbol{d}(\boldsymbol{x}_d, t)\|.$$

Figure 4b gives a measure of the tightness of the two bounds, calculated as the percentage difference with respect to the actual deviation.

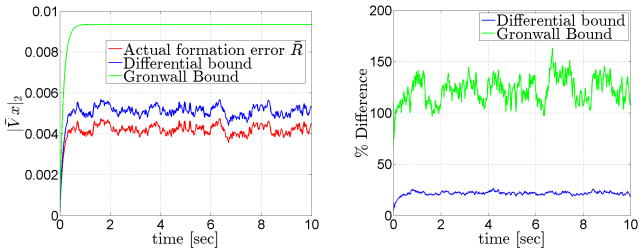

(a) Comparison for $\|\boldsymbol{\delta}_z\|$. (b) Bound tightness

Fig. 4: Tightness for robustness bounds.

The simulation was carried out for 6 robots, with look-ahead horizon $N = 2$. Based on the chosen cyclic control gains, $\Lambda = -6.928$ and $\bar{d} = 0.065$. From Figure 4b, we can see that, on average, the differential equation bound overestimates the actual deviation by about 30% while the Gronwall bound is even more conservative.

VI. Conclusions

In this paper we studied distributed control algorithms for 3D formations, ranging from regular polygon to Johnson solid formations. These algorithms are desirable for their simplicity, in that they only require relative position measurements and an agreement between the robots on the desired orientation in space. For second order dynamics, the requirements extend to include relative and absolute velocities. Our approach was to leverage the mathematical properties of cyclic pursuit along with results from contraction and partial contraction theory. Furthermore, we studied the robustness of cyclic controllers under bounded additive disturbances and provided performance bounds with respect to the formation error.

This work allows several possible avenues for extension. First, it would be useful to extend the use of partial contraction theory to analyze convergence to more general formations such as ellipses. This could be accomplished using linear transformations on the constraints and the cyclic controller. Additionally, analyzing the effects of control saturation on system convergence is a vital prerequisite to implementation on actual hardware. This might involve, for instance, imposing either hard nonlinearities on the controller output or embedding the output within a smooth bounded function. It is also of interest to evaluate optimality properties of cyclic controllers by introducing an objective cost function to be minimized and using it to guide gain selection and/or look-ahead horizon. Finally, we would like to explore opportunities to implement such algorithms for space and underwater applications.

References

[1] W. Sheng, Q. Yang, T. J, and N. Xi, "Distributed multi-robot coordination in area exploration," *Robotics and Autonomous Systems*, vol. 54, no. 12, pp. 945 – 955, 2006.

[2] R. Smith and F. Hadaegh, "Control topologies for deep space formation flying spacecraft," in *American Control Conference*, vol. 4, 2002, pp. 2836–2841.

[3] F. Arrichiello, H. Heidarsson, S. Chiaverini, and G. Sukhatme, "Cooperative caging using autonomous aquatic surface vehicles," in *Proc. IEEE Conf. on Robotics and Automation*, May 2010, pp. 4763–4769.

[4] A. Jadbabaie, J. Lin, and A. Morse, "Coordination of groups of mobile autonomous agents using nearest neighbor rules," *IEEE Transactions on Automatic Control*, vol. 48, no. 6, pp. 988–1001, June 2003.

[5] J. Lawton, R. Beard, and B. Young, "A decentralized approach to formation maneuvers," *IEEE Transactions on Robotics and Automation*, vol. 19, no. 6, pp. 933–941, Dec 2003.

[6] W. Ren and R. Beard, "Decentralized scheme for spacecraft formation flying via the virtual structure approach," *AIAA Journal of Guidance, Control, and Dynamics*, vol. 27, no. 1, pp. 73–82, Jan-Feb 2004.

[7] J. Marshall, "Coordinated autonomy: Pursuit formations of multivehicle systems," Ph.D. dissertation, University of Toronto, 2005.

[8] J. Chen, D. Sun, J. Yang, and H. Chen, "Leader-follower formation control of multiple non-holonomic mobile robots incorporating a receding-horizon scheme," *International Journal of Robotics Research*, vol. 29, no. 6, pp. 727–747, 2010.

[9] L. Consolini, F. Morbidi, D. Prattichizzo, and M. Tosques, "Leader follower formation control of nonholonomic mobile robots with input constraints," *Automatica*, vol. 44, no. 5, pp. 1343 – 1349, 2008.

[10] D. P. Scharf, F. Y. Hadaegh, and S. R. Ploen, "A survey of spacecraft formation flying guidance and control, part II: Control," in *American Control Conference*, vol. 4, Boston, MA, Jun. 2004, pp. 2976–2985.

[11] Y. Cao, W. Yu, W. Ren, and G. Chen, "An overview of recent progress in the study of distributed multi-agent coordination," *IEEE Transactions on Industrial Informatics*, vol. 9, no. 1, pp. 427–438, Feb 2013.

[12] J. Marshall, M. Broucke, and B. Francis, "Formations of vehicles in cyclic pursuit," *IEEE Transactions on Automatic Control*, vol. 49, no. 11, pp. 1963–1974, Nov 2004.

[13] M. Pavone and E. Frazzoli, "Decentralized policies for geometric pattern formation and path coverage," *ASME Journal on Dynamic Systems, Measurement, and Control*, vol. 129, no. 5, pp. 633–643, 2007.

[14] J. L. Ramirez, M. Pavone, E. Frazzoli, and D. W. Miller, "Distributed Control of Spacecraft Formations via Cyclic Pursuit: Theory and Experiments," *AIAA Journal of Guidance, Control, and Dynamics*, vol. 33, no. 5, pp. 1655–1669, 2010.

[15] J. Ramirez-Riberos and J. Slotine, "Contraction theory approach to generalized decentralized cyclic algorithms for global formation acquisition and control," in *Proc. IEEE Conf. on Decision and Control*, Dec 2012.

[16] W. Lohmiller and J. Slotine, "On contraction analysis for non-linear systems," *Automatica*, vol. 34, no. 6, pp. 683 – 696, 1998.

[17] Q. Pham, N. Tabareau, and J. Slotine, "A contraction theory approach to stochastic incremental stability," *IEEE Transactions on Automatic Control*, vol. 54, no. 4, pp. 816–820, April 2009.

[18] W. Wang and J. Slotine, "On partial contraction analysis for coupled nonlinear oscillators," *Biological Cybernetics*, vol. 92, no. 1, pp. 38–53, 2005.

[19] Q. Pham and J. Slotine, "Stable concurrent synchronization in dynamic system networks," *Neural Networks*, pp. 62–77, 2007.

[20] O. Wallner, K. Ergenzinger, and R. Flatscher, "X-array aperture configuration in planar or non-planar spacecraft formation for darwin/tpf-i candidate architectures," in *Proceedings of SPIE 6693, Techniques and Instrumentation for Detection of Exoplanets III*, Sep 2007.

[21] J. Jouffroy and J. Slotine, "Methodological remarks on contraction theory," in *Proc. IEEE Conf. on Decision and Control*, vol. 3, Dec 2004, pp. 2537–2543 Vol.3.

[22] R. Gray, "Toeplitz and circulant matrices: A review," Tech. Rep., 2001.

[23] T. H. Gronwall, "Note on the derivatives with respect to a parameter of the solutions of a system of differential equations," *Annals of Mathematics*, vol. 20, no. 4, pp. pp. 292–296, 1919.

[24] J.-J. E. Slotine and W. Li, *Applied Nonlinear Control*. Prentice Hall, 1991.

APPENDIX

A. Mathematic Preliminaries

1) Kronecker Product: Let A and B be matrices of size $m \times n$ and $p \times q$ respectively. The Kronecker product of A and B is defined as:

$$A \otimes B = \begin{bmatrix} a_{11}B & \cdots & a_{1n}B \\ \vdots & & \vdots \\ a_{m1}B & \cdots & a_{mn}B \end{bmatrix},$$

where $A \otimes B$ has dimensions $mp \times nq$. if λ_A is an eigenvalue of A with eigenvector $\mathbf{v_A}$, and similarly λ_B and $\mathbf{v_B}$ are an eigenvalue and eigenvector pair for B then the corresponding eigenvalue and eigenvector pair for $A \otimes B$ is $\lambda_A \lambda_B$ and $\mathbf{v_A} \otimes \mathbf{v_B}$. Furthermore, we also note the following identity: $(A \otimes B)(C \otimes D) = AC \otimes BD$, where the products AC and BD are defined.

2) Eigenvalues and Eigenvectors of Circulant Matrices: From [22], the eigenvalues of a circulant matrix are the Discrete Fourier Transform of the first row of the circulant matrix.

Theorem VI.1 (Adapted from Theorem 3.1 in [22])**.** *Every circulant matrix C has eigenvectors:*

$$\mathbf{v_k} = \frac{1}{\sqrt{n}}(1, e^{-2\pi j(k-1)/n}, \ldots, e^{-2\pi j(k-1)(n-1)/n})^T, \quad k = 1, 2, \ldots, n, \tag{28}$$

and corresponding eigenvalues:

$$\lambda_k = \sum_{p=0}^{n-1} c_p e^{2\pi j(k-1)p/n}, \tag{29}$$

and can be expressed in the form $C = U\Lambda U^*$ where U is a unitary matrix with the k^{th} column equal to the k^{th} eigenvector and Λ is a diagonal matrix of corresponding eigenvalues. Note that the same matrix U diagonalizes all circulant matrices. Thus if C and B are $n \times n$ circulant matrices, with eigenvalues $\{\lambda_{B,k}\}_{k=1}^n$ and $\{\lambda_{C,k}\}_{k=1}^n$ respectively, then:

1) *C and B commute ($CB = BC$) and CB is also a circulant matrix with eigenvalues equal to $\{\lambda_{B,k}\lambda_{C,k}\}_{k=1}^n$*
2) *$C + B$ is also circulant with eigenvalues $\{\lambda_{B,k} + \lambda_{C,k}\}_{k=1}^n$*

B. Proofs

Proof of Lemma III.1. Necessity is trivial. We then consider sufficiency. First, we prove that constraints (4a) and (4b) ensure that all robots lie in a common plane, i.e.,

$$\boldsymbol{e}_z^T \boldsymbol{x}_i = a, \tag{30}$$

for all $i \in \{1, \ldots, n\}$ and some $a \in \mathbb{R}$. Since $\boldsymbol{e}_z$ is a left eigenvector of $R_{2\pi/n}$, with eigenvalue equal to 1, the rotational constraints imply $\boldsymbol{e}_z^T(\boldsymbol{x}_{i+1} - \boldsymbol{x}_i) = \boldsymbol{e}_z^T(\boldsymbol{x}_{i+2} - \boldsymbol{x}_{i+1})$, for $i = 1, \ldots, n-2$. Combining this set of equations with the in-plane constraint, one can write

$$\boldsymbol{e}_z^T(\boldsymbol{x}_{i+1} - \boldsymbol{x}_i) = \boldsymbol{e}_z^T(\boldsymbol{x}_{i+2} - \boldsymbol{x}_{i+1}),$$

for $i = 1, \ldots, n-1$ and where the indices are modulo n. One can then readily show that

$$\boldsymbol{e}_z^T \boldsymbol{x}_{i+2} = \boldsymbol{e}_z^T \boldsymbol{x}_2 + i\, \boldsymbol{e}_z^T(\boldsymbol{x}_2 - \boldsymbol{x}_1), \tag{31}$$

for $i = 1, \dots, n-1$ and where the indices are modulo n. Hence, for $i = n-1$, one obtains

$$\boldsymbol{e}_z^T \boldsymbol{x}_1 = \boldsymbol{e}_z^T \boldsymbol{x}_2 + (n-1)\, \boldsymbol{e}_z^T (\boldsymbol{x}_2 - \boldsymbol{x}_1),$$

which implies that $\boldsymbol{e}_z^T(\boldsymbol{x}_2 - \boldsymbol{x}_1) = \mathbf{0}$. Hence, by setting $\boldsymbol{e}_z^T \boldsymbol{x}_2 := a$, one immediately obtains equation (30). We have then proven that all robots lie in a common plane. Now, for n points lying in a common plane, the rotational constraints represent the definition of a regular polygon.

For independence, we note that each successive rotational constraint involves at least one robot that does not belong to any of the previous constraints, proving that the rotational constraints are independent. Then, the in-plane constraint is necessary to ensure that the robots do not form a spiral formation out of the desired plane, thereby reducing the dimensionality of the solution subspace. Thus, the in-plane constraint must be independent to the rotational constraints. □

Proof of Corollary III.2. Necessity is straightforward. We then consider sufficiency. To prove the claim, we need to show that the rotational constraints are sufficient to ensure that all robots lie in the desired plane for $j = 1, \dots, n$. The claim then follows directly. Now, the rotational constraints imply

$$\boldsymbol{e}_z^T(\boldsymbol{x}_{i+1} - \boldsymbol{x}_i) = \boldsymbol{e}_z^T(\boldsymbol{x}_{i+2} - \boldsymbol{x}_{i+1}), \tag{32}$$

for $i = 1, \dots, n-2$. For two robots with indices j and $j+1$ that lie in the desired plane, we know that $\boldsymbol{e}_z^T \boldsymbol{x}_j = \boldsymbol{e}_z^T \boldsymbol{x}_{j+1} = a \in \mathbb{R}$. Thus, for $j = 1, \dots, n-1$, we can recursively use (32) to show

$$\boldsymbol{e}_z^T \boldsymbol{x}_i = \boldsymbol{e}_z^T \boldsymbol{x}_j, \tag{33}$$

for $i = 1, \dots, n$. For the case where $j = n$, we have:

$$\boldsymbol{e}_z^T \boldsymbol{x}_n = \boldsymbol{e}_z^T \boldsymbol{x}_1.$$

However, we note that (31) still holds for $i = 1, \dots, n-2$ using the rotational constraints alone. Then, setting $i = n-2$, we obtain

$$(\boldsymbol{e}_z^T \boldsymbol{x}_n - \boldsymbol{e}_z^T \boldsymbol{x}_1) + (n-1)\boldsymbol{e}_z^T(\boldsymbol{x}_2 - \boldsymbol{x}_1) = (n-1)\boldsymbol{e}_z^T(\boldsymbol{x}_2 - \boldsymbol{x}_1),$$

which gives $\boldsymbol{e}_z^T \boldsymbol{x}_2 = \boldsymbol{e}_z^T \boldsymbol{x}_1$. We can now again use (32) recursively to show (33), completing the proof.

□

Proof of Lemma III.4. Equations (4a) and (4b) can be written in matrix form as $V\,\boldsymbol{x} = \mathbf{0}$, where

$$V = \begin{bmatrix} I_3 & -(I_3 + R_{2\pi/n}) & R_{2\pi/n} & & \\ 0_{3\times 3} & I_3 & -(I_3 + R_{2\pi/n}) & & \\ \vdots & \vdots & \vdots & \cdots & \\ \boldsymbol{e}_z^T R_{2\pi/n} & 0_{1\times 3} & 0_{1\times 3} & & \end{bmatrix} \begin{bmatrix} 0_{3\times 3} & \cdots & \cdots & 0_{3\times 3} \\ R_{2\pi/n} & 0_{3\times 3} & \cdots & \vdots \\ \vdots & \vdots & \vdots & \vdots \\ \cdots & \cdots & \boldsymbol{e}_z^T & -\boldsymbol{e}_z^T(I_3 + R_{2\pi/n}) \end{bmatrix}. \tag{34}$$

Simplifying the above expression, one obtains

$$\begin{aligned} V =& \mathcal{W}_n \mathrm{circ}[I_3, -I_3, 0_{3\times 3}, \dots, 0_{3\times 3}] + \\ & \mathcal{W}_n \mathrm{circ}[0_{3\times 3}, -R_{2\pi/n}, R_{2\pi/n}, 0_{3\times 3}, \dots, 0_{3\times 3}] \\ =& \mathcal{W}_n(L_1 \otimes I_3) + \mathcal{W}_n((L_1 - L_2) \otimes R_{2\pi/n} I_3) \\ =& \mathcal{W}_n \left(L_1 I_n \otimes I_3 I_3 + (L_1 - L_2) I_n \otimes R_{2\pi/n} I_3\right) \\ =& \mathcal{W}_n (L_1 \otimes I_3 + (L_1 - L_2) \otimes R_{2\pi/n})(I_n \otimes I_3), \end{aligned} \tag{35}$$

where the last equality follows from the properties of the Kronecker product. The claim then follows. □

Proof of Lemma III.5. Note that the rotational constraints in (4a) and the in-plane constraint (4b) define the subspace, $\mathcal{M}_n$ to be a regular polygon with normal $\boldsymbol{e}_z$. The following analysis therefore assumes that all robots lie in a single plane and satisfy the rotational constraints. Then,

$$\begin{aligned} \dot{\boldsymbol{x}}_{i+1} - \dot{\boldsymbol{x}}_i =& \sum_{m=1}^{N} k_m(\boldsymbol{x}, t) \big[R_m(\boldsymbol{x}, t)(\boldsymbol{x}_{i+1+m} - \boldsymbol{x}_{i+1}) \\ & + R_m^T(\boldsymbol{x}, t)(\boldsymbol{x}_{i+1-m} - \boldsymbol{x}_{i+1}) \big] \\ & - \sum_{m=1}^{N} k_m(\boldsymbol{x}, t) \big[R_m(\boldsymbol{x}, t)(\boldsymbol{x}_{i+m} - \boldsymbol{x}_i) \\ & + R_m^T(\boldsymbol{x}, t)(\boldsymbol{x}_{i-m} - \boldsymbol{x}_i) \big]. \end{aligned} \tag{36}$$

Now by the constraints described by (4a), we can state:

$$\begin{aligned} \boldsymbol{x}_{i+1+m} - \boldsymbol{x}_{i+1} &= R_{2\pi/n}(\boldsymbol{x}_{i+2+m} - \boldsymbol{x}_{i+2}), \text{ and} \\ \boldsymbol{x}_{i+1-m} - \boldsymbol{x}_{i+1} &= R_{2\pi/n}(\boldsymbol{x}_{i+2-m} - \boldsymbol{x}_{i+2}). \end{aligned}$$

Thus, the first term in (36) can be written as:

$$\begin{aligned} \dot{\boldsymbol{x}}_{i+1} =& \sum_{m=1}^{N} k_m(\boldsymbol{x}, t) \big[R_m R_{2\pi/n}(\boldsymbol{x}, t)(\boldsymbol{x}_{i+2+m} - \boldsymbol{x}_{i+2}) \\ & + R_m^T R_{2\pi/n}(\boldsymbol{x}, t)(\boldsymbol{x}_{i+2-m} - \boldsymbol{x}_{i+2}) \big] \\ =& R_{2\pi/n} \sum_{m=1}^{N} k_m(\boldsymbol{x}, t) \big[R_m(\boldsymbol{x}, t)(\boldsymbol{x}_{i+2+m} - \boldsymbol{x}_{i+2}) \\ & + R_m^T(\boldsymbol{x}, t)(\boldsymbol{x}_{i+2-m} - \boldsymbol{x}_{i+2}) \big] \\ =& R_{2\pi/n} \dot{\boldsymbol{x}}_{i+2}, \end{aligned} \tag{37}$$

where the order of R_m and $R_{2\pi/n}$ can be swapped since they are rotation matrices about the same axis. Similarly, it can be shown that $\dot{\boldsymbol{x}}_i = R_{2\pi/n} \dot{\boldsymbol{x}}_{i+1}$. Thus, rewriting (36):

$$\dot{\boldsymbol{x}}_{i+1} - \dot{\boldsymbol{x}}_i = R_{2\pi/n}(\dot{\boldsymbol{x}}_{i+2} - \dot{\boldsymbol{x}}_{i+1}).$$

To prove the arbitrary normal case, simply replace R_m and $R_{2\pi/n}$ with their similarity transformed versions with respect to $R_\eta \neq I_3$. □

Proof of Theorem III.6. We provide the proof for the general case where the desired formation plane is not necessarily the horizontal plane. The proof leverages the following lemma.

Lemma VI.2. *Given a symmetric matrix $\mathcal{X}$ such that $\mathcal{X} \prec 0$, then $\mathcal{W}_n \mathcal{X} \mathcal{W}_n^T \prec 0$.*

Proof. If $\mathcal{X} \prec 0$ then $\lambda_{max}(\mathcal{X}) < 0$. Noting that $\mathcal{W}_n$ is sub-unitary, by the Cauchy Interlacing theorem, $\lambda_{max}(\mathcal{W}_n \mathcal{X} \mathcal{W}_n^T) \leq \lambda_{max}(\mathcal{X}) < 0$. □

The proof of the theorem then simply expands upon the convergence conditions expressed in (8).

Given the results of Lemma VI.2, we only need to consider the uniform negative-definiteness of the inner term (not involving $\mathcal{W}_n$) in (8). For the scenario where the desired formation plane is not the horizontal $x-y$ plane, by the discussion in Remark III.9, we use the similarity transformed versions of the projection matrix V and the cyclic controller and show that it has no effect on the resulting analysis.

From (10) and (11), we begin by noting that $\mathcal{P}_n \mathcal{R}_\eta \mathcal{L}_{m\eta} \mathcal{R}_\eta^T \mathcal{P}_n^T = \mathcal{P}_n \mathcal{L}_m \mathcal{P}_n^T$ since $\mathcal{L}_{m\eta} = \mathcal{R}_\eta^T \mathcal{L}_m \mathcal{R}_\eta$. Thus, the analysis does not depend on the arbitrary choice

of the orientation of the desired plane normal in the global coordinate system.

Now, given the matrices $\mathcal{P}_n$ and $\mathcal{L}_m$ are $\in \mathcal{C}_{L\otimes R}$, they have the same set of eigenvectors. Then, for any eigenvector $\boldsymbol{v}_i$ in this set, we have the following relation for the corresponding eigenvalues:

$$\lambda_i\left(\mathcal{P}_n\mathcal{L}_m\mathcal{P}_n^T\right) = \lambda_i(\mathcal{P}_n)\lambda_i(\mathcal{P}_n^T)\lambda_i(\mathcal{L}_m).$$

To derive the eigenvalues of $\mathcal{P}_n$, we note that $\mathcal{P}_n = L_1 \otimes I_3 + (L_1 - L_2) \otimes R_{2\pi/n}$ which is the sum of two $\mathcal{C}_{L\otimes R}$ matrices and thus the eigenvalues of $\mathcal{P}_n$ must be the sum of the eigenvalues of $L_1 \otimes I_3$ and $(L_1 - L_2) \otimes R_{2\pi/n}$. From Theorem VI.1, we have the general result:

$$\lambda_i(L_m) = 1 - e^{\frac{2m\pi}{n}(i-1)j},\ i = 1, \ldots, n. \tag{38}$$

Additionaly from Theorem VI.1, the eigenvalues of $L_1 - L_2$ are the sum of eigenvalues of L_1 and $-L_2$. The eigenvalues of $R_{2\pi/n}$ are $\{1, e^{\pm\frac{2\pi}{n}j}\} = e^{\frac{2k\pi}{n}j}$ where $k \in \{-1, 0, 1\}$. Thus, the eigenvalues of $\mathcal{P}_n$ and $\mathcal{P}_n^T$ are the set $i \in \{1, \ldots, n\}, k \in \{-1, 0, 1\}$:

$$\begin{aligned}\lambda(\mathcal{P}_n, \mathcal{P}_n^T) = &\left(1 - e^{\pm\frac{2\pi}{n}(i-1)j}\right)\\ &+ \left(e^{\pm\frac{4\pi}{n}(i-1)j} - e^{\pm\frac{2\pi}{n}(i-1)j}\right)e^{\pm\frac{2k\pi}{n}j},\end{aligned} \tag{39}$$

where the positive and negative signs are for $\mathcal{P}_n$ and $\mathcal{P}_n^T$ respectively. In a similar fashion, the eigenvalues for $\mathcal{L}_m$ are:

$$\begin{aligned}\lambda(\mathcal{L}_m) =& \left(1 - e^{\frac{2m\pi}{n}(i-1)j}\right)e^{k\alpha_m j}\\ &+ \left(1 - e^{\frac{-2m\pi}{n}(i-1)j}\right)e^{-k\alpha_m j}\\ =&2\left(\cos(k\alpha_m) - \cos\left(k\alpha_m + \frac{2\pi m(i-1)}{n}\right)\right).\end{aligned} \tag{40}$$

Multiplying (39) and (40) gives the expression for $\lambda\left(\mathcal{P}_n\mathcal{L}_m\mathcal{P}_n^T\right) = \lambda_{ik}^{(m)}(\boldsymbol{x}, t)$. To obtain the summation form in (9), note that $\mathcal{P}_n\mathcal{L}_m\mathcal{P}_n^T \in \mathcal{C}_{L\otimes R}$ for all m. Thus $\lambda\left(\mathcal{P}_n \sum_{m=1}^{N} k_m\mathcal{L}_m\mathcal{P}_n^T\right) = \sum_{m=1}^{N} k_m\left[\lambda\left(\mathcal{P}_n\mathcal{L}_m\mathcal{P}_n^T\right)\right]$. Having obtained the summation form, (9) follows directly from trying to show (8) given Lemma VI.2.

□

Proof of Lemma IV.3. We proceed by induction. Let $\boldsymbol{\mathcal{F}_k} = \{\mathcal{F}_1, \ldots, \mathcal{F}_k\}$ denote a partial list of faces, constrained by the set of equations $[V^{(k)}]\boldsymbol{x} = \boldsymbol{0}$, where $[V^{(k)}] = \begin{bmatrix}V^{(1)^T} & \ldots & V^{(k)^T}\end{bmatrix}^T$, $k \leq L$. Similarly, let $[\tilde{V}^{(k)}] = \begin{bmatrix}\tilde{V}^{(1)^T} & \ldots & \tilde{V}^{(k)^T}\end{bmatrix}^T$.

Base case: $k = 2$: It is clear that $\mathcal{N}\left([V^{(2)}]\right) = \mathcal{N}([\tilde{V}^{(2)}])$ as $[V^{(2)}] = [\tilde{V}^{(2)}]$. To see that $[V^{(2)}]$ is full row-rank, we note that $V^{(1)}$ is full row-rank (Lemma III.1) and each successive rotational constraint within $V^{(2)}$ (counting around the polygon starting from the shared edge) involves at least one robot that does not belong to any previous constraints in $V^{(1)}$ or $V^{(2)}$. The in-plane constraint for $V^{(2)}$ further reduces the dimension of the solution set by constraining the rotational degree of freedom for $\mathcal{F}_1$: there is only one orientation of $\mathcal{F}_1$ (up to normal parity) under which the edge shared by the two faces is orthogonal to $\boldsymbol{n}_2$. Therefore all constraints in $[V^{(2)}]$ are independent.

Hypothesis: Assume that the set of equations $[\tilde{V}^{(k)}]\boldsymbol{x} = \boldsymbol{0}$ and $[V^{(k)}]\boldsymbol{x} = \boldsymbol{0}$ are equivalent and that $[V^{(k)}]$ is full row-rank.

We now prove that $[\tilde{V}^{(k+1)}]\boldsymbol{x} = \boldsymbol{0}$ and $[V^{(k+1)}]\boldsymbol{x} = \boldsymbol{0}$ are also equivalent and that $[V^{(k+1)}]$ is full row-rank. By the inductive hypothesis, $[\tilde{V}^{(k)}]\boldsymbol{x} = \boldsymbol{0}$ ensures that $\boldsymbol{\mathcal{F}_k}$ is defined and as a direct consequence of Remark IV.1 and Lemma IV.2, the faces have a fixed orientation consistent with their position within the polyhedron.

Now, from our labeling convention, $\mathcal{F}_{k+1}$ must share exactly one edge (i.e. exactly 2 robots) with a face within $\boldsymbol{\mathcal{F}_k}$, and that the edge must lie in a plane normal to $\boldsymbol{n}_{k+1}$. The tree structure of $\mathcal{F}_L$ prevents any additional shared edges. From Corollary III.2, the rotational constraints encoded in $V^{(k+1)}$ are indeed sufficient to form $\mathcal{F}_{k+1}$. Furthermore, as the shared edge between $\mathcal{F}_{k+1}$ and $\boldsymbol{\mathcal{F}_k}$ is fixed in space, the constraints $V^{(k+1)}$ also ensure that $\mathcal{F}_{k+1}$ does not possess any rotational degree of freedom within its plane and therefore, must possess an orientation consistent with its position within the polyhedron. Thus, $[V^{(k+1)}]\boldsymbol{x} = \boldsymbol{0}$ and $[\tilde{V}^{(k+1)}]\boldsymbol{x} = \boldsymbol{0}$ are equivalent.

To see that $[V^{(k+1)}]$ is full row rank, we note that each successive rotational constraint within $V^{(k+1)}$ involves at least one robot not represented by any of the existing constraints within $[V^{(k)}]$ or $V^{(k+1)}$. Then, by similar reasoning as for the base case, all constraints in $[V^{(k+1)}]$ are independent.

By induction, both claims are proven.

□

Proof of Theorem V.1. Starting from (26), $\boldsymbol{\delta_x} = (\bar{V}^T\bar{V} + \bar{U}^T\bar{U})\boldsymbol{\delta_x} = \bar{V}^T\boldsymbol{\delta_z} + \bar{U}^T\bar{U}\boldsymbol{\delta_x}$. Now, $\bar{U}^T\bar{U}\boldsymbol{\delta_x} \in \mathcal{M}_n$, so $\bar{V}\mathcal{L}\left(\bar{U}^T\bar{U}\ \boldsymbol{\delta_x}\right) = \boldsymbol{0}$. Thus,

$$\dot{\boldsymbol{\delta}}_{\boldsymbol{z}}(t) = -\bar{V}\mathcal{L}\bar{V}^T\boldsymbol{\delta_z} + \boldsymbol{d}(\boldsymbol{x}_d, t).$$

Pre-multiplying by $2\boldsymbol{\delta_z}(t)$ we obtain:

$$2\boldsymbol{\delta_z}^T\dot{\boldsymbol{\delta}}_{\boldsymbol{z}} = \frac{d(\boldsymbol{\delta_z}^T\boldsymbol{\delta_z})}{dt} = -2\boldsymbol{\delta_z}^T\left(\bar{V}\mathcal{L}\bar{V}^T\right)\boldsymbol{\delta_z} + 2\boldsymbol{\delta_z}^T\boldsymbol{d}(\boldsymbol{x}_d, t).$$

Letting $\bar{R}^2 = \boldsymbol{\delta_z}^T\boldsymbol{\delta_z}$, one can write

$$\frac{d\bar{R}^2}{dt} = 2\bar{R}\frac{d\bar{R}}{dt} = -2\boldsymbol{\delta_z}^T\left(\bar{V}\mathcal{L}\bar{V}^T\right)\boldsymbol{\delta_z} + 2\boldsymbol{\delta_z}^T\boldsymbol{d}(\boldsymbol{x}_d, t).$$

Noting that:

$$-\boldsymbol{\delta_z}^T\left(\bar{V}\mathcal{L}\bar{V}^T\right)\boldsymbol{\delta_z} \leq -\lambda_{\min}\left(\bar{V}\mathcal{L}\bar{V}^T\right)\boldsymbol{\delta_z}^T\boldsymbol{\delta_z} = \Lambda\bar{R}^2,$$

and

$$\boldsymbol{\delta_z}^T\boldsymbol{d}(\boldsymbol{x}_d, t) \leq \|\boldsymbol{\delta_z}\|\|\boldsymbol{d}(\boldsymbol{x}_d, t)\| = \bar{R}\|\boldsymbol{d}(\boldsymbol{x}_d, t)\|,$$

we get:

$$\bar{R}\dot{\bar{R}} \leq \Lambda\bar{R}^2 + \bar{R}\|\boldsymbol{d}(\boldsymbol{x}_d, t)\|.$$

Thus,

$$\dot{\bar{R}} \leq \Lambda\bar{R} + \|\boldsymbol{d}(\boldsymbol{x}_d, t)\|, \tag{41a}$$

$$\leq \Lambda\bar{R} + \bar{d} \tag{41b}$$

By using Gronwall's Lemma [23], the claim follows. □

C. Control over Formation Size

By setting $|\alpha_m| = m\pi/n$, the formation converges to a regular polygon of fixed, but uncontrolled size. As a natural extension of this approach, [15] introduces an additive term to the control law to control the size of the formation. The subsequent analysis for proving convergence however, is inconsistent with the method of partial contraction theory. We present an alternative algorithm for controlling formation size and in addition, the center of the formation that only leverages the property of flow-invariant subspaces. Assume zero internal dynamics $\boldsymbol{g}(\boldsymbol{x})$. The algorithm is split into two phases:

1) Phase 1: Apply the symmetric cyclic controller in (6) with $\alpha_m = m\pi/n$ until the robots converge within some error bound of the desired formation, as measured by the residual of cyclic controller.
2) Phase 2: Apply the flow-invariant formation size and center controllers in order to converge to a polygon with desired inter-robot distance ρ and center $\boldsymbol{x}_c$.

To determine the switch from Phase 1 to Phase 2, a simple decentralized algorithm can be implemented whereby each robot evaluates the residual of its own symmetric cyclic controller which is known to converge to zero when the robots are in formation. Once all robots have sufficiently converged to $\mathcal{M}_n$, consider the following control law:

$$\boldsymbol{u}_i = f_s(z_i(\boldsymbol{x}))(\boldsymbol{x}_{i+1} - \boldsymbol{x}_i) + k_c \left(\boldsymbol{x}_c - \frac{1}{n}\sum_{i=1}^{n} \boldsymbol{x}_i \right), \qquad (42)$$

where $z_i(\boldsymbol{x}) = \|\boldsymbol{x}_{i+1} - \boldsymbol{x}_i\| - \rho$, ρ is the desired inter-robot neighbor distance in the formation, f_s is an odd scalar function that operates on the error in inter-robot distance satisfying the property $z f_s(z) > 0$; k_c is the geometric center control gain and $\boldsymbol{x}_c$ is the desired geometric center. Here $\|(\cdot)\|$ denotes the Euclidean norm.

The size controller acts only between robots i and $i+1$, modulo n while the formation center controller uses the offset of the current geometric center from the desired center and computes compensation in this direction which is applied equally to all robots. In order to compute the current geometric center of the formation in a decentralized fashion, we only require a single robot to know its global position. The geometric center can then be calculated extremely quickly via two successive message passes, the first to iteratively compute the geometric center using relative positions between robots, and the second to distribute this value amongst all robots.

Define $\mathcal{M}_{n\rho}$ to be a subset of the original invariant subspace $\mathcal{M}_n$, corresponding to the space of regular polygon formations with inter-robot neighbor distance equal to ρ. Thus,

$$\mathcal{M}_{n\rho} = \{\boldsymbol{x} : \boldsymbol{x} \in \mathcal{M}_n \wedge \|\boldsymbol{x}_{i+1} - \boldsymbol{x}_i\| = \rho\}.$$

To prove convergence to this subspace, we first start with a lemma to prove that the subspace, $\mathcal{M}_n$ is indeed flow-invariant with respect to (42).

Lemma VI.3. *The subspace $\mathcal{M}_n$ is flow-invariant with respect to the dynamics given in* (42).

Proof. It is straightforward to see that the formation center controller is invariant to $\mathcal{M}_n$.

Now, for $\boldsymbol{x} \in \mathcal{M}_n$, $f_s(z_i(\boldsymbol{x}))$ is the same for all robots. Let this value be equal to $\bar{f}_s$. The global size control vector $\boldsymbol{u}_s$ can then be written as:

$$\boldsymbol{u}_s = -\bar{f}_s(L_1 \otimes I_3)\boldsymbol{x}.$$

Thus, $V\,\boldsymbol{u}_s = -\bar{f}_s\,V\,(L_1 \otimes I_3)\,\boldsymbol{x} = \boldsymbol{0}$, proving the claim. □

Having shown that $\mathcal{M}_n$ is flow invariant with respect to the augmented dynamics, the proof to show convergence to the subspace, $\mathcal{M}_{n\rho}$ is presented in [15] and leverages the results of LaSalle's Invariant Set Theorem [24].

Finally, to see that the center of the formation converges to the desired center $\boldsymbol{x}_c$, note that for $\boldsymbol{x} \in \mathcal{M}_n$:

$$\frac{d}{dt}\|\boldsymbol{x}_c - \frac{1}{n}\sum_{i=1}^{n}\boldsymbol{x}_i\| = -\frac{(\boldsymbol{x}_c - \frac{1}{n}\sum_{i=1}^{n}\boldsymbol{x}_i)^T}{\|\boldsymbol{x}_c - \frac{1}{n}\sum_{i=1}^{n}\boldsymbol{x}_i\|}(\frac{1}{n}\sum_{i=1}^{n}\dot{\boldsymbol{x}}_i).$$

Now $\dot{\boldsymbol{x}}_i$ is given by the sum of the size and center controllers. However, by symmetry, the sum of the size controller over all robots must equal 0 when $\boldsymbol{x} \in \mathcal{M}_n$. The summation then simply equals $nk_c(\boldsymbol{x}_c - \frac{1}{n}\sum_{i=1}^{n}\boldsymbol{x}_i)$. Thus, we obtain:

$$\frac{d}{dt}\|\boldsymbol{x}_c - \frac{1}{n}\sum_{i=1}^{n}\boldsymbol{x}_i\| = -k_c\|\boldsymbol{x}_c - \frac{1}{n}\sum_{i=1}^{n}\boldsymbol{x}_i\|.$$

For $k_c > 0$, the center of the formation converges to the desired center $\boldsymbol{x}_c$.

D. Control Effort for Symmetric Cyclic Controller

In complement to the the 3D trajectories and inter-robot distances plots presented in the main body of this paper, the following plot exemplifies the reduction in control effort by using a larger look-ahead horizon. For this simulation, we neglect the formation size and center controllers, focusing only on convergence to a planar polygon. In order to draw comparisons, we maintain the same absolute convergence rate upper bound, i.e. $\lambda_{\min}\left(\bar{V}\mathcal{L}\bar{V}\right)$ while varying the look-ahead horizon and gains. The plot shows the Euclidean norm of the net cyclic controller, that is $\|\mathcal{L}\boldsymbol{x}(t)\|_2$ for 6 robots starting at the same initial conditions.

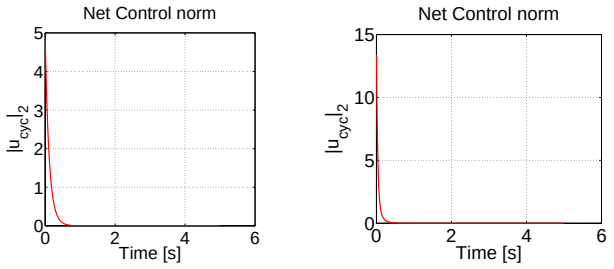

(a) Control norm with $N = 2$, $k_m = 2$ (b) Control norm with $N = 1$, $k_m = 6.928$

Fig. 5: Comparison of control effort with varying gains and look-ahead horizon

From the plot we can immediately note a drastic reduction in control effort for the case with $N = 2$. Indeed, the peak control norm for the case with $N = 1$ and higher gains is more than 2.5 times higher than for the controller with $N = 2$ and smaller gains.